LETTER

doi:10.1038/nature15768

Type-II Weyl semimetals

Alexey A. Soluyanov[1], Dominik Gresch[1], Zhijun Wang[2], QuanSheng Wu[1], Matthias Troyer[1], Xi Dai[3] & B. Andrei Bernevig[2]

Fermions—elementary particles such as electrons—are classified as Dirac, Majorana or Weyl. Majorana and Weyl fermions had not been observed experimentally until the recent discovery of condensed matter systems such as topological superconductors and semimetals, in which they arise as low-energy excitations[1–6]. Here we propose the existence of a previously overlooked type of Weyl fermion that emerges at the boundary between electron and hole pockets in a new phase of matter. This particle was missed by Weyl[7] because it breaks the stringent Lorentz symmetry in high-energy physics. Lorentz invariance, however, is not present in condensed matter physics, and by generalizing the Dirac equation, we find the new type of Weyl fermion. In particular, whereas Weyl semimetals—materials hosting Weyl fermions—were previously thought to have standard Weyl points with a point-like Fermi surface (which we refer to as type-I), we discover a type-II Weyl point, which is still a protected crossing, but appears at the contact of electron and hole pockets in type-II Weyl semimetals. We predict that WTe_2 is an example of a topological semimetal hosting the new particle as a low-energy excitation around such a type-II Weyl point. The existence of type-II Weyl points in WTe_2 means that many of its physical properties are very different to those of standard Weyl semimetals with point-like Fermi surfaces.

The band structure of some metals has non-trivial topological features[2]. Of such metals, the ones with vanishingly small density of states at the Fermi level—semimetals—stand out. For these materials, a distinction between topologically protected surface states and bulk metallic states can be made and their Fermi surfaces can be topologically characterized, unlike the case for metals, which have many states at the Fermi level. Two kinds of topological semimetals have attracted special attention: Dirac and Weyl semimetals. In these materials, a linear crossing of two (Weyl) or four (Dirac) bands occurs at the Fermi level (see Fig. 1a). The effective Hamiltonian for these crossings is given by the Weyl or gapless-Dirac equation, respectively. The Weyl crossings are protected from gapping, owing to the massless nature of the Weyl fermion. In the following, we limit the discussion to Weyl crossings only, although our results also hold for Dirac crossings.

The appearance of Weyl points (WPs) is possible only if the product of parity and time reversal is not a symmetry of the structure. When present, a WP acts as a topological charge—either a source or a sink of Berry curvature. A Fermi surface enclosing a WP has a well-defined Chern number, corresponding to the topological charge of this WP. Because the net charge must vanish in the entire Brillouin zone, WPs always come in pairs; they are stable to weak perturbations and are annihilated only in pairs of opposite charge. A large number of unusual physical phenomena are associated with Weyl topological semimetals, including the existence of open Fermi arcs in the surface Fermi surface[1,8] and various magnetotransport anomalies[9–15].

Weyl semimetals with broken time-reversal symmetry have been predicted to exist in several materials[1,16,17], but these predictions have yet to be experimentally verified. More recently, the Weyl semimetal was predicted to exist in inversion-breaking single-crystal nonmagnetic materials of the TaAs class[3,4]; this prediction has since been verified experimentally[5,6].

Weyl semimetals were previously thought to have a point-like Fermi surface at the WP. We refer to these as type-I WPs (WP1s), to distinguish them from the new type-II WPs (WP2s) that exist at the boundaries between electron and hole pockets, as illustrated in Fig. 1b. We discuss general conditions for WP2s to appear, and present evidence that WTe_2—the material with the largest never-saturating magnetoresistance reported[18] so far—is an example of the new type of topological semimetal hosting eight WP2s. These WP2s come in two quartets located 0.052 eV and 0.058 eV above the Fermi level. We present topological arguments that prove the existence of the new topological semimetal phase in WTe_2. We provide evidence of doping-driven topological Lifshitz transitions, which are characteristic of WP2s, as well as emerging Fermi arcs in the surface Fermi surface.

We start by considering the most general Hamiltonian describing a WP

$$H(\boldsymbol{k}) = \sum_{\substack{i=x,y,z \\ j=0,x,y,z}} k_i A_{ij} \sigma_j$$

where $\boldsymbol{k}$ is the wave vector in reciprocal space (crystal momentum vector), A is a 3×4 matrix of coefficients, σ_0 is the 2×2 unit matrix and and $\sigma_j, j = x, y, z$ are the three Pauli matrices. The energy spectrum is

$$\varepsilon_{\pm}(\boldsymbol{k}) = \sum_{i=x,y,z} k_i A_{i0} \pm \sqrt{\sum_{j=x,y,z} \left(\sum_{i=x,y,z} k_i A_{ij} \right)^2} = T(\boldsymbol{k}) \pm U(\boldsymbol{k}) \quad (1)$$

where $T(\boldsymbol{k})$ and $U(\boldsymbol{k})$ can be considered as the kinetic and potential components of the energy spectrum. $T(\boldsymbol{k})$, which is linear in momentum, tilts the cone-like spectrum $\varepsilon_{\pm}(\boldsymbol{k})$. This tilt breaks the Lorentz invariance of Weyl fermions in quantum field theory, but was previously considered unimportant. However, because Lorentz invariance does not need to be respected in condensed matter, its inclusion is important and leads to a finer classification of distinct Fermi surfaces, in correspondence with the theory of quadric surfaces, which suggests that there are exactly two distinct types of WPs (see Supplementary Information).

If, for a particular direction in reciprocal space, T is dominant over U, the tilt becomes large enough to cause a WP to appear at the point where the open electron and hole pockets touch, contrary to the standard case of a point-like Fermi surface. Thus, the condition for a WP to be of type II is that there exists a direction $\hat{\boldsymbol{k}}$ for which $T(\hat{\boldsymbol{k}}) > U(\hat{\boldsymbol{k}})$. If such a direction does not exist, then the WP is of type I. The clear qualitative distinction between the Fermi surfaces of the two types of WPs leads to marked differences in the thermodynamics of the hosting materials and their response to magnetic fields. In particular, in contrast to a WP1, which exhibits a chiral anomaly[9] for any direction of the magnetic field, the chiral anomaly appears in a WP2 only when the direction of the magnetic field is within a cone where $|T(\boldsymbol{k})| > |U(\boldsymbol{k})|$. If the field direction is outside this cone, then the Landau-level spectrum is gapped and has no chiral zero mode (see Supplementary Information).

On the lattice, the 'no-go' theorem[19] guarantees that Weyl fermions appear in pairs with Chern numbers of opposite sign. Because the

[1]Theoretische Physik and Station Q Zurich, ETH Zurich, 8093 Zurich, Switzerland. [2]Department of Physics, Princeton University, Princeton, New Jersey 08544, USA. [3]Institute of Physics, Chinese Academy of Sciences, Beijing 100190, China.

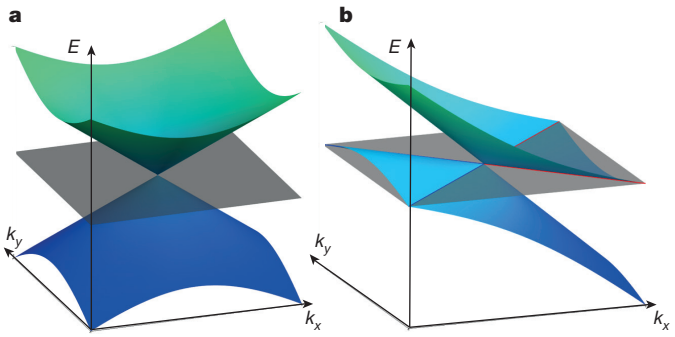

Figure 1 | Possible types of Weyl semimetals. a, Type-I WP with a point-like Fermi surface. **b**, A type-II WP appears as the contact point between electron and hole pockets. The grey plane corresponds to the position of the Fermi level, and the blue (red) lines mark the boundaries of the hole (electron) pockets.

Chern number of a WP is not changed by $T(\boldsymbol{k})$, WPs of different type can be chiral/anti-chiral partners of each other. The number of WPs of a certain type can be odd, but the total number of WPs must be even (for example, there can be one WP1 and one WP2).

We now describe WTe_2, a material we identified to host the new WPs. The crystal structure of WTe_2 is orthorhombic with space group $Pmn2_1$ (C_{2v}^7). Its primitive unit cell contains four formula units. The atomic structure is layered, with single layers of W separated from each other by Te bilayers and stacked along the z axis (see Supplementary Information). The distance between adjacent W atoms is considerably smaller along the x axis than it is along the y or z axes, creating strong anisotropy. The unit cell has two reflection symmetries: a mirror in the y–z plane m_{yz} and a glide plane g_{xz} formed by a reflection in the x–z plane followed by a translation by (0.5, 0, 0.5). Combined, they form a non-symmorphic twofold rotation C_2 (that is, a twofold rotation that is combined with a translation by a fraction of a lattice constant), which is important in the following symmetry arguments.

The result of band-structure calculations (see Supplementary Information) without spin–orbit coupling (SOC) is shown in Fig. 2a along the Γ–X direction, where an intermediate point $\Sigma = (0.375, 0, 0)$ is introduced. In addition to electron and hole pockets, 16 WPs per spin are found in WTe_2 in the absence of SOC (not shown in Fig. 2a). Half of these points occur at points of low symmetry with $k_z \neq 0$; the other half appear in the $k_z = 0$ plane, where the product of time reversal and C_2 ($C_{2T} = C_2T$) forms a little group. Generically, degeneracies on high-symmetry planes are forbidden; however, owing to the C_{2T} symmetry, twofold degeneracies are locally stable at points in the $k_z = 0$ plane. On the Γ–X line, the spectrum is generally gapped with a bandgap of approximately 1 meV, separating valence and conduction bands; see Fig. 2a.

Accounting for spin, but without SOC, bands become doubly degenerate, owing to opposite spin projections. This degeneracy doubles the topological charge of each WP because, by SU(2) symmetry, WPs corresponding to opposite spins have identical topological charge. Infinitesimal SOC cannot gap these WPs, giving a general criterion by which to search for Weyl semimetals: WPs are first found without SOC on the high-symmetry planes; the effects of SOC on these WPs are studied separately.

In WTe_2 SOC is not small. When turned on, it preserves electron and hole pockets, but substantially changes the structure of WPs. At intermediate SOC, WPs move, emerging or annihilating in pairs of opposite chirality. At full SOC, all WPs with $k_z \neq 0$ are annihilated. In the $k_z = 0$ plane, double degeneracies at isolated k points are still allowed by symmetry. Eight such gapless points are found, formed by the topmost valence and lowest conduction bands at full SOC. A pair of such points is shown in Fig. 2c. The other three pairs are related to this one by reflections. Energetically, both points are located only slightly (0.052 eV and 0.058 eV) above the Fermi energy E_F; see Supplementary Information for details.

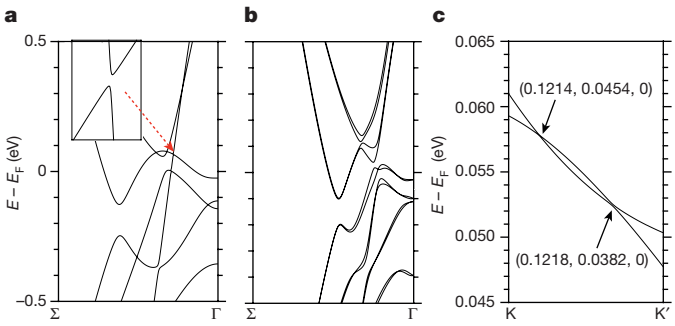

Figure 2 | Band structure of WTe_2. a, Band structure of WTe_2 without SOC. A fraction of the Γ–X segment is shown: the point Σ has coordinates (0.375, 0, 0). A bandgap of approximately 1 meV is shown in the inset, signalling a gapless point nearby. **b**, Band structure of WTe_2 with SOC. **c**, One of the four pairs of WPs is shown along the line K–K′, where K = (0.1208, 0.0562, 0) and K′ = (0.1226, 0.0238, 0). Their locations are designated in reduced coordinates (in units of reciprocal lattice constants).

Establishing degeneracies of bands (and the existence of WPs) computationally (or by inspection) is prone to finite-size effects: a point thought to be a degeneracy point might turn out to have a minuscule gap upon increasing computational precision. To rigorously establish the presence of WPs, we performed many tests that involve computing topological indices. The topological charge (±1) of each WP was found using an extension of the Wilson-loop and hybrid-Wannier-centres methods[20,21] to type-II Weyl semimetals. $\mathbb{Z}_2$ topological indices were also computed on several planes (including those in both standard and non-standard geometries) in the Brillouin zone. In total, these tests not only proved the existence of WPs, but also elucidated the structure of the Berry-flux connection between WPs and of the Fermi arcs on the surface of WTe_2. The resultant Fermi-arc structure is consistent with the calculations presented below. A detailed description of topological indices and ways to obtain them are found in Supplementary Information.

To check the nature of the WPs, we obtained the energy spectrum around them from first-principles calculations and fitted it to the theoretical model derived by symmetry analysis (Supplementary Information). Considering only linear terms in k_i—the momentum relative to the position of the WP—the spectrum in equation (1) becomes

$$\varepsilon_{\pm}(\boldsymbol{k}) = Ak_x + Bk_y \pm \sqrt{e^2k_z^2 + (ak_x + ck_y)^2 + (bk_x + dk_y)^2}$$

The values of the parameters A, B, a, b, c, d and e are given in the Supplementary Information. The kinetic component of the energy dominates along the line connecting this WP to its nearest neighbour (see Fig. 2c and Supplementary Information). We thus conclude that WTe_2 is a type-II Weyl semimetal.

We now discuss the Fermi surface topology and possible topological Lifshitz transitions in WTe_2. The evolution of the Fermi surface obtained from first-principles calculations is shown in Fig. 3 for different values of E_F. Owing to reflection symmetries, only part of the $k_z = 0$ plane of the Fermi surface is shown. For $E_F = 0$ eV, the Fermi surface is formed of two pairs of electron pockets and two pairs of hole pockets (eight pockets in total), which are separated in momentum space. For each pair, the larger pocket completely encloses the smaller one, in agreement with experiments[22]. This property is illustrated in Fig. 3a, where four halved pockets (two electron and two hole) are shown. The other halves are obtained by the glide reflection g_{xz}, and the remaining four pockets with $k_x > 0$ are obtained by the mirror reflection m_{yz}. All Fermi surfaces have zero Chern numbers when $E_F = 0$.

When E_F is raised, two additional electron pockets appear; the previously existing electron pockets persist. The hole pockets shrink quickly, two disappearing completely. Each of the remaining two split into two disconnected pockets. As a result, there are six electron pockets and four hole pockets in total (see Fig. 3b). When the Fermi level

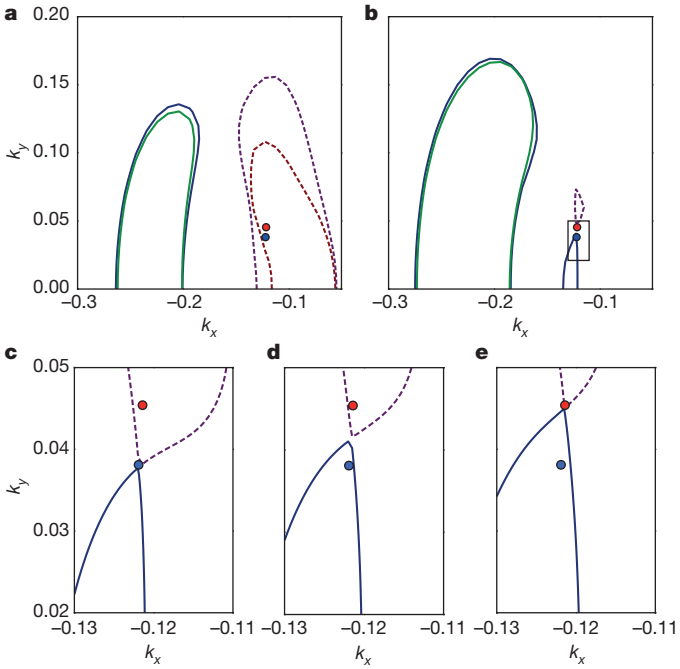

Figure 3 | Fermi surface at $k_z = 0$. A part of the Brillouin zone is shown. **a**, $E_F = 0$ eV; electron pockets (blue and green solid lines) and hole pockets (red and magenta dashed lines) come in pairs. WP with Chern number +1 (−1) is shown in red (blue). **b**, The representative structure of electron and hole pockets at higher energies ($E_F = 0.055$ eV shown). There are four hole pockets (one shown; dashed magenta line) and six electron pockets (halves of three of them shown; blue and green solid lines). The boxed region is the region shown in **c**–**e** for different values of E_F. **c**, $E_F = 0.052$ eV is set to the lower-energy WP. Contact between electron and hole pockets occurs at this WP. **d**, $E_F = 0.055$ eV is set to be between the two WPs. The electron and hole pockets are disconnected. The hole pocket encloses a WP with a Chern number $C = +1$. The electron pocket encloses the WP with $C = -1$ and its mirror image (not shown); the net Chern number of this pocket is zero. **e**, When $E_F = 0.058$ eV is set to the higher-energy WP, electron and hole pockets touch again (shown). They reopen at larger E_F with zero Chern numbers.

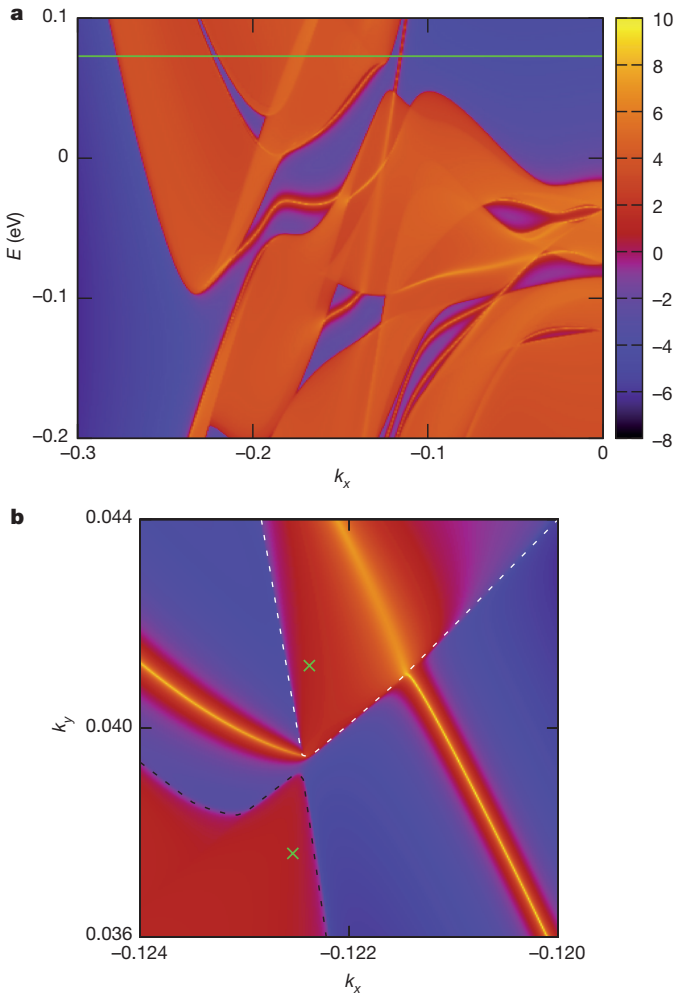

Figure 4 | Topological surface states. a, Spectral function of the (001) surface. The Fermi level (green line) is set to be between the WPs. **b**, Fermi surface of the (001) surface and a Fermi arc connecting hole and electron pockets. Green crosses mark the positions of WPs.

is tuned to the first WP, $E_F = 0.052$ eV (corresponding to the addition of approximately 0.064 electrons per unit cell), each of the two newly appeared electron pockets touches two hole pockets at the positions of the WPs, as illustrated in Fig. 3c for part of $k_z = 0$ plane. Further increase of E_F disconnects the electron and hole pockets again—see Fig. 3d for $E_F = 0.055$ eV—but with changed topology: electron pockets still have zero Chern numbers because they enclose two WPs of opposite charge, related by g_{xz}. The hole pockets have Chern numbers of ± 1. Topologies of the other hole pockets are obtained by changing the sign of the Chern number according to the appropriate mirror and glide symmetries. The pockets touch again (see Fig. 3e) when the Fermi level is tuned to the higher-energy WP, $E_F = 0.058$ eV (corresponding to approximately 0.079 additional electrons per unit cell). Upon raising E_F further, the pockets disconnect again, and all Fermi-surface Chern numbers become zero.

To facilitate the observation of topological Lifshitz transitions, hydrostatic pressure is applied. Neighbouring WPs are pushed away from each other in k space under compression. In particular, a 0.5% (2%) compression increases the distance between the WPs from 0.7% to 2% (4%) of the reciprocal vector $|\boldsymbol{G}_2|$ (see Supplementary Information for a discussion of strain effects, including how to obtain only four WPs).

Finally, we discuss the topological surface states of WTe_2. Owing to reflection symmetries, WPs of opposite chirality are projected on top of each other on the (100) and (010) surfaces, which hence do not exhibit topologically protected surface states.

For the (001) surface, all the WPs project onto distinct points; hence, topological surface states appear. When E_F is tuned to be between the WPs, the hole pocket has non-zero Chern number and a Fermi arc emerges from it, connecting it to the WP of opposite Chern number inside the electron pocket. Figure 4a illustrates the spectral function of the (001) surface, where surface states connecting electron and hole bands are clearly visible. The Fermi surface of this surface has a topological Fermi arc (Fig. 4b) connecting projections of the topological hole (Fig. 3c–e) and electron pockets. The other surface state crossing the hole pocket emerges from the electron pocket (not seen in Fig. 4) and goes back into it, and thus can be pushed into the continuum of bulk states (see Supplementary Information).

Of other transition metal dichalcogenides, another strong candidate material is $MoTe_2$ (ref. 23), which is reported to be a semimetal resembling pressurized WTe_2. This material can also be used to explore new physical phenomena arising in the new topological semimetal phase presented here.

Received 1 June; accepted 22 September 2015.

1. Wan, X., Turner, A. M., Vishwanath, A. & Savrasov, S. Y. Topological semimetal and Fermi-arc surface states in the electronic structure of pyrochlore iridates. *Phys. Rev. B* **83,** 205101 (2011).
2. Volovik, G. E. *The Universe in a Helium Droplet* (Oxford Univ. Press, 2009).
3. Weng, H., Fang, C., Fang, Z., Bernevig, B. A. & Dai, X. Weyl semimetal phase in noncentrosymmetric transition-metal monophosphides. *Phys. Rev. X* **5,** 011029 (2015).
4. Huang, S.-M. *et al.* An inversion breaking Weyl semimetal state in the TaAs material class. *Nature Commun.* **6,** 7373 (2015).
5. Xu, S.-Y. *et al.* Discovery of a Weyl fermion semimetal and topological Fermi arcs. *Science* **349,** 613–617 (2015).

6. Lv, B. Q. *et al.* Experimental discovery of Weyl semimetal TaAs. *Phys. Rev. X* **5,** 031013 (2015).
7. Weyl, H. Elektron und Gravitation. *I. Z. Phys.* **56,** 330–352 (1929).
8. Silaev, M. A. & Volovik, G. E. Topological Fermi arcs in superfluid ^{3}He. *Phys. Rev. B* **86,** 214511 (2012).
9. Nielsen, H. B. & Ninomiya, M. The Adler–Bell–Jackiw anomaly and Weyl fermions in a crystal. *Phys. Lett. B* **130,** 389–396 (1983).
10. Zyuzin, A. A. & Burkov, A. A. Topological response in Weyl semimetals and the chiral anomaly. *Phys. Rev. B* **86,** 115133 (2012).
11. Hosur, P. & Qi, X. Recent developments in transport phenomena in Weyl semimetals. *C. R. Phys.* **14,** 857–870 (2013).
12. Volovik, G. E. Kopnin force and chiral anomaly. *JETP Lett.* **98,** 753–757 (2014).
13. Zhang, C. *et al.* Observation of the Adler–Bell–Jackiw chiral anomaly in a Weyl semimetal. Preprint at http://arXiv.org/abs/1503.02630 (2015).
14. Xiong, J. *et al.* Signature of the chiral anomaly in a Dirac semimetal: a current plume steered by a magnetic field. Preprint at http://arXiv.org/abs/1503.08179 (2015).
15. Huang, X. *et al.* Observation of the chiral-anomaly-induced negative magnetoresistance in 3D Weyl semimetal TaAs. *Phys. Rev. X* **5,** 031023 (2015).
16. Xu, G., Weng, H., Wang, Z., Dai, X. & Fang, Z. Chern semimetal and the quantized anomalous Hall effect in $HgCr_2Se_4$. *Phys. Rev. Lett.* **107,** 186806 (2011).
17. Burkov, A. A. & Balents, L. Weyl semimetal in a topological insulator multilayer. *Phys. Rev. Lett.* **107,** 127205 (2011).
18. Ali, M. N. *et al.* Large, non-saturating magnetoresistance in WTe_2. *Nature* **514,** 205–208 (2014).
19. Nielsen, H. B. & Ninomiya, M. Absence of neutrinos on a lattice: (I). Proof by homotopy theory. *Nucl. Phys. B* **185,** 20–40 (1981).
20. Soluyanov, A. A. & Vanderbilt, D. Computing topological invariants without inversion symmetry. *Phys. Rev. B* **83,** 235401 (2011).
21. Yu, R., Qi, X. L., Bernevig, A., Fang, Z. & Dai, X. Equivalent expression of $\mathbb{Z}_2$ topological invariant for band insulators using the non-Abelian Berry connection. *Phys. Rev. B* **84,** 075119 (2011).
22. Pletikosić, I., Ali, M. N., Fedorov, A. V., Cava, R. J. & Valla, T. Electronic structure basis for the extraordinary magnetoresistance in WTe_2. *Phys. Rev. Lett.* **113,** 216601 (2014).
23. Brown, B. E. The crystal structures of WTe_2 and high-temperature $MoTe_2$. *Acta Crystallogr.* **20,** 268–274 (1966).

Supplementary Information is available in the online version of the paper.

Acknowledgements A.A.S., D.G., QS.W. and M.T. acknowledge the support of Microsoft Research, the Swiss National Science Foundation through the National Competence Center in Research MARVEL and the European Research Council through ERC Advanced Grant SIMCOFE. Z.W. and B.A.B. acknowledge the support of ARO MURI W911NF-12-1-0461, ONR-N00014-11-1-0635, NSF CAREER DMR-0952428, NSF MRSEC DMR-0819860, the Packard Foundation and a Keck grant. X.D. is supported by the National Natural Science Foundation of China, the 973 program of China (no. 2011CBA00108 and no. 2013CB921700) and the "Strategic Priority Research Program (B)" of the Chinese Academy of Sciences (no. XDB07020100).

Author Contributions All authors contributed to performing the calculations and the analysis of the results.

Author Information Reprints and permissions information is available at www.nature.com/reprints. The authors declare no competing financial interests. Readers are welcome to comment on the online version of the paper. Correspondence and requests for materials should be addressed to A.A.S. (soluyanov@itp.phys.ethz.ch).